Study of neutrino mass matrices with vanishing trace and one vanishing minor

Sangeeta Dey[*] and Mahadev Patgiri[†]
Department of Physics, Cotton University, Guwahati 781001, India

(Received 9 February 2022; accepted 5 January 2023; published 13 February 2023)

In this paper we carry out a systematic texture study of the neutrino mass matrix with the Ansätze—(i) one vanishing minor and (ii) the zero sum of the mass eigenvalues with the CP phases (henceforth vanishing trace). There are six possible textures of a neutrino mass matrix with one vanishing minor. The viability of each texture is checked with 3σ values of current neutrino data by drawing scatter plots. In our analysis we are motivated to use the ratio of solar to atmospheric mass-squared differences R_ν for its precise measurement (and also the atmospheric mixing angle θ_{23}) to constrain phenomenologically first the Dirac CP phase δ in the range of 0°–360° for a given texture with the solutions of the constraint equations. Subsequently we employ this constrained δ to determine the range of completely unknown Majorana CP phases (α and β) for all the viable textures. We also check the neutrinoless double beta decay rate $|m_{ee}|$ and the Jarlskog invariant J_{cp} for the textures. Finally the symmetry realization of all the viable textures under the flavor symmetry group Z_5 via seesaw mechanism is implemented along with the FN mechanism to determine mass hierarchy structure.

DOI: 10.1103/PhysRevD.107.035012

I. INTRODUCTION

The phenomenon of neutrino oscillations, i.e., the change from one flavor to another has been decisively confirmed by the results of the neutrino oscillation experiments carried out for the last few decades. The neutrino oscillation theory predicts massive neutrinos and flavor mixing. Many neutrino oscillation experiments [1–5] have entered the regime of precision measurement of the three mixing angles $(\theta_{12}, \theta_{23}, \theta_{13})$ and two mass-squared differences $(\Delta m^2_{12}, \Delta m^2_{23})$. The ordering of neutrino masses is not yet known but can be probed in the experiments, viz., the JUNO experiment [6], long baseline experiment with the Hyper-Kamiokande detector and J-PARK accelerator [7], and DUNE experiment [8]. The absolute scale of neutrinos is also not yet experimentally known, but the information about the upper bounds obtained from the KATRIN [9], GERDA [10], EXO [11], and KamLAND-ZEN [12] experiments and some cosmological observations indicate the sub-eV scale.

Theoretical understanding of the origin of such small neutrino masses and large mixings is a very important issue to be addressed in the leptonic sector of particle physics. In the three neutrino flavor scheme, the neutrinos are described by a symmetric 3×3 mass matrix M_ν which is diagonalized by the Pontecorvo-Maki-Nakagawa-Sakata (PMNS) mixing matrix, $V_{\rm PMNS}$ giving the mass eigenvalues of light neutrinos. The textures of the effective neutrino mass matrix have been investigated with different proposals in the literature, e.g., the vanishing minors [13–19], zero elements [20–30], equality of elements/minors [31–34], zero trace [35,36], zero determinant [37], etc., that are phenomenologically viable in light of the current neutrino data. Such texture study restricts the possible structures of neutrino mass matrix and also reduces the free parameters. From the point of model building, this approach is useful and economical. Again, the canonical seesaw mechanism is a simple and theoretically appealing framework beyond the Standard Model of particle physics to generate tiny masses and large mixing of observable neutrinos. In this framework, M_ν is built from two more fundamental mass matrices: (i) the Dirac neutrino mass matrix M_D and (ii) the heavy right-handed Majorana neutrino mass matrix M_R. We adopt a principle that any texture of M_ν acquired is a result of the combined effect of the textures of M_D and M_R via the canonical seesaw formula. The lepton sector is not yet completely known. In the seesaw framework, neutrinos would be completely described by three masses (m_1, m_2, m_3), three mixing angles $(\theta_{12}, \theta_{13}, \theta_{23})$, one Dirac CP phase δ, and two Majorana CP phases (α, β). Currently we have the experimental data on two mass-squared differences and hence the ratio of these two mass-squared differences R_ν, three mixing angles, the strength of CP violation, the Jarlskog invariant J_{CP}, and the

[*]phy1891006_sangeeta@cottonuniversity.ac.in
[†]mahadevpatgiri@cottonuniversity.ac.in

neutrinoless double beta decay rate $|m_{ee}|$. Now in phenomenology, the texture study of M_ν maybe a useful tool for predicting values of the other unknown parameters on the basis of currently available data. Such conditions on M_ν theoretically indicate some underlying flavor symmetry and hence the origin of such textures becomes important in model building.

In the present work we intend to explore the texture of neutrino mass matrices with two Ansätze imposing simultaneously: (i) one vanishing minor and (ii) the zero sum of the mass eigenvalues with the CP phases [38]; henceforth it will be termed as the vanishing trace. The following are the primary motivations of considering these two Ansätze in our work:

(a) In seesaw mechanism neutrino mass matrix is given by $M_\nu = -M_D M_R^{-1} M_D^T$ obtained from the Dirac mass matrix M_D and the heavy right-handed Majorana mass matrix M_R which are considered to be more fundamental. Now the zeros in M_D and M_R propagate to M_ν and manifest as its vanishing minor(s) or texture zero(s) via the seesaw formula. On the other hand, the zeros in M_D and M_R represent the underlying flavor symmetry that may be realized by the discrete symmetry group Z_N [39,40]. These Z_N are a subgroup of the $U(1)$ Abelian gauge group, which gives a strong theoretical foundation in this approach.

(b) Some of the nonoscillation experiments, viz., neutrinoless double beta decay, tritium beta decay end point spectrum, etc., can measure the absolute mass scale directly, whereas the oscillation experiments can measure the mass-squared differences of neutrinos known as solar and atmospheric mass splittings, and ordering of neutrino masses. It is also noted that authors in their paper [41] showed that the traceless condition enabled one to calculate the absolute masses of neutrinos in the normal hierarchy (NH) or in the inverted hierarchy (IH) mass pattern from the current neutrino data.

We have six possible textures of M_ν each having one vanishing minor and vanishing trace. Each texture has two simultaneous constraint equations in two variables defined from the ratio of mass eigenvalues with CP phases. With the solutions we plot R_ν (and also θ_{23}) versus δ to check the viability of the particular texture. The 3σ values of R_ν and θ_{23} either restrict a texture to the subrange of δ out of the full range 0°–360° or completely rule it out. Then we explore the range of Majorana CP phases by plotting α and β against the allowed range of δ for viable cases. The viability of those allowed textures are further checked in the light of $|m_{ee}|$ and J_{cp}. The successful textures in our proposed investigations are subject to the symmetry realization under the flavor group Z_5 in the seesaw mechanism which is further augmented by the Froggatt-Nielsen (FN) mechanism [42,43] to know the mass pattern.

The paper is organized as follows: In Sec. II, we present the framework of the neutrino mass matrix having one vanishing minor and vanishing trace, followed by the texture analysis in Sec. III. In Sec. IV we have done the symmetry realization of viable textures. Finally we present results and discussion in Sec. V.

II. NEUTRINO MASS MATRIX FRAMEWORK

At first we consider the neutrino mass matrix M_ν as

$$M_\nu = V \begin{pmatrix} m_1 & 0 & 0 \\ 0 & m_2 & 0 \\ 0 & 0 & m_3 \end{pmatrix} V^T, \tag{1}$$

where (m_1, m_2, m_3) are the neutrino mass eigenvalues and V is the diagonalizing PMNS matrix with the following parametrization [44] in the basis of the diagonal charged-lepton mass matrix:

$$V = UP_\nu = \begin{pmatrix} c_{12}c_{13} & c_{13}s_{12} & s_{13}e^{-i\delta} \\ -s_{12}c_{23} - c_{12}s_{13}s_{23}e^{i\delta} & c_{12}c_{23} - s_{12}s_{13}s_{23}e^{i\delta} & c_{13}s_{23} \\ s_{23}s_{12} - c_{12}c_{23}s_{13}e^{i\delta} & -c_{12}s_{23} - c_{23}s_{12}s_{13}e^{i\delta} & c_{13}c_{23} \end{pmatrix} \mathrm{diag}(1, e^{i\alpha}, e^{i(\beta+\delta)}), \tag{2}$$

where $(\theta_{12}, \theta_{23}, \theta_{13})$ are the solar, atmospheric, and reactor mixing angles, respectively; δ is the Dirac CP phase; and α, β are the Majorana CP phases.

Now we can recast the neutrino mass matrix in the following strategic form:

$$M_\nu = U \begin{pmatrix} \lambda_1 & 0 & 0 \\ 0 & \lambda_2 & 0 \\ 0 & 0 & \lambda_3 \end{pmatrix} U^T, \tag{3}$$

where $\lambda_1 = m_1$, $\lambda_2 = m_2 e^{2i\alpha}$, $\lambda_3 = m_3 e^{2i(\beta+\delta)}$. Now using Eq. (3) any element of the neutrino mass matrix M_ν can be expressed as

$$(M_\nu)_{mn} = \sum_{i=1}^{3} U_{mi} U_{ni} \lambda_i. \tag{4}$$

The cofactors of the off diagonal elements of the symmetric matrix M_ν can be written in the following form,

$$C_{mn} = (-1)^{m+n}((M_\nu)_{(m+1,n-1)}(M_\nu)_{(m+2,n+1)} - (M_\nu)_{(m+1,n+1)}(M_\nu)_{(m+2,n+2)}), \tag{5}$$

and that for diagonal elements can be written as

$$C_{mm} = (-1)^{2m}((M_\nu)_{(m+1,m+1)}(M_\nu)_{(m+2,m+2)} - (M_\nu)_{(m+1,m+2)}(M_\nu)_{(m+2,m+1)}). \quad (6)$$

For $m+l$, $n+l>3$, we have to take the values $(m+l)-3$, $(n+l)-3$. Here m, n can take values (1, 2, 3), and $l=1, 2$. Now we impose the condition for vanishing minor, i.e.,

$$C_{mn}=0, \qquad C_{mm}=0. \quad (7)$$

Solving Eq. (7) we get

$$m_1 m_2 e^{2i\alpha} A_3 + m_2 m_3 e^{2i(\alpha+\beta+\delta)} A_1 + m_3 m_1 e^{2i(\beta+\delta)} A_2 = 0, \quad (8)$$

where

$$A_i = (U_{pj}U_{qj}U_{rk}U_{sk} - U_{tj}U_{uj}U_{vk}U_{wk}) + (j \leftrightarrow k); \quad (9)$$

here (i, j, k) is a cyclic permutation of (1, 2, 3). Therefore the two constraint equations are

$$\lambda_1\lambda_2 A_3 + \lambda_2\lambda_3 A_1 + \lambda_3\lambda_1 A_2 = 0, \quad (10)$$

$$\lambda_1 + \lambda_2 + \lambda_3 = 0. \quad (11)$$

Considering $\lambda_1 > 0$ and defining $X = \frac{\lambda_2}{\lambda_1}$ and $Y = \frac{\lambda_3}{\lambda_1}$, Eqs. (10) and (11) become

$$XA_3 + XYA_1 + YA_2 = 0, \quad (12)$$

$$1 + X + Y = 0. \quad (13)$$

Solving Eqs. (12) and (13) we get the following ratios:

$$X_\pm = \frac{(A_3 - A_1 - A_2) \pm \sqrt{(A_3 - A_1 - A_2)^2 - 4A_1A_2}}{2A_1}, \quad (14)$$

$$Y_\pm = \frac{(A_2 - A_1 - A_3) \pm \sqrt{(A_3 - A_1 - A_2)^2 - 4A_1A_2}}{2A_1}. \quad (15)$$

For the solution pairs (X_+, Y_-) and (X_-, Y_+) we get the Majorana phases as

$$\alpha = \frac{1}{2}\mathrm{Arg}\left[\frac{(A_3 - A_1 - A_2) \pm \sqrt{(A_3 - A_1 - A_2)^2 - 4A_1A_2}}{2A_1}\right], \quad (16)$$

$$\beta = \frac{1}{2}\mathrm{Arg}\left[\frac{(A_2 - A_1 - A_3) \pm \sqrt{(A_3 - A_1 - A_2)^2 - 4A_1A_2}}{2A_1}\right] e^{-2i\delta}. \quad (17)$$

The other two solution pairs (X_+, Y_+) and (X_-, Y_-) satisfy the constraint equations under the condition $(A_3 - A_1 - A_2)^2 - 4A_1A_2 = 0$. For these two solution pairs we have the Majorana phases as

$$\alpha = \frac{1}{2}\mathrm{Arg}\left[\frac{(A_3 - A_1 - A_2)}{2A_1}\right];$$
$$\beta = \frac{1}{2}\mathrm{Arg}\left[\frac{(A_2 - A_1 - A_3)}{2A_1}\right] e^{-2i\delta}. \quad (18)$$

The ratios of the neutrino masses

$$\rho = \left|\frac{m_2}{m_1} e^{2i\alpha}\right| \quad (19)$$

and

$$\sigma = \left|\frac{m_3}{m_1} e^{2i\beta}\right| \quad (20)$$

are related to the ratio of solar and atmospheric mass-squared differences

$$R_\nu = \frac{\delta m^2}{\Delta m^2} = \frac{2(\rho^2 - 1)}{|2\sigma^2 - \rho^2 - 1|}, \quad (21)$$

where $\delta m^2 = m_2^2 - m_1^2$ is called the solar mass splitting and $\Delta m^2 = |m_3^2 - \frac{1}{2}(m_2^2 + m_1^2)|$ the atmospheric mass splitting. For NH, the ratio $R_\nu = \frac{2\epsilon}{\sigma^2}$, if we consider $\rho = 1 + \epsilon$ for m_1 and m_2 being very close to each other with the values $0.013 < \epsilon < 0.017$ on 3σ range. For IH, $R_\nu = \frac{2(\rho^2-1)}{\rho^2+1}$. From the 3σ values of Δm^2_{21} and $|\Delta m^2_{3l}|$ we obtain the range $R_\nu = (0.026\text{–}0.035)$ (refer to Table I).

The measure of CP violation, i.e., the Jarlskog invariant [45] is given by

$$J_{CP} = \frac{1}{8}\sin 2\theta_{12}\sin 2\theta_{23}\sin 2\theta_{13}\cos\theta_{13}\sin\delta. \quad (22)$$

The nature of the neutrino is still unknown whether it is the Dirac or the Majorana type. The observation of neutrinoless double beta decay would indicate the process of the lepton number violation and confirm the Majorana nature of neutrinos. The rate of neutrinoless double beta decay depends on the effective Majorana mass of the electron neutrino:

$$|m_{ee}| = |m_1 c_{12}^2 c_{13}^2 + m_2 s_{12}^2 c_{13}^2 e^{2i\alpha} + m_3 s_{13}^2 e^{2i\beta}|. \quad (23)$$

Various ongoing and upcoming neutrinoless double beta decay experiments such as CUORICINO [46], CUORE [47], GERDA [10], MAJORANA [48], SuperNEMO [49], EXO [11], and GENIUS [50] aim to achieve a sensitivity up to 0.01 eV for $|m_{ee}|$. The most constraint upper limit

TABLE I. Current neutrino oscillation parameters from global fits [51]. Here $\Delta m^2_{3l} = \Delta m^2_{31} > 0$ for normal hierarchy and $\Delta m^2_{3l} = \Delta m^2_{32} < 0$ for inverted hierarchy.

	Normal ordering		Inverted ordering	
Parameter	Best fit $\pm 1\sigma$	3σ range	Best fit $\pm 1\sigma$	3σ range
θ°_{12}	$33.45^{+0.77}_{-0.75}$	31.27–35.86	$33.45^{+0.78}_{-0.75}$	31.27–35.87
θ°_{23}	$42.1^{+1.1}_{-0.9}$	39.7–50.9	$49.0^{+0.9}_{-1.3}$	39.8–51.6
θ°_{13}	$8.62^{+0.12}_{-0.12}$	8.25–8.98	$8.61^{+0.14}_{-0.12}$	8.24–9.02
δ°_{cp}	230^{+36}_{-25}	144–350	278^{+22}_{-30}	194–345
$\Delta m^2_{21}/10^{-5}$ eV^2	$7.42^{+0.21}_{-0.20}$	6.82–8.04	$7.42^{+0.21}_{-0.20}$	6.82–8.04
$\lvert\Delta m^2_{3l}\rvert/10^{-3}$ eV^2	$2.510^{+0.027}_{-0.027}$	2.430–2.593	$2.490^{+0.026}_{-0.028}$	-2.574 to -2.410

has been set to $|m_{ee}| < 0.061$–0.165 eV at 90% CL by the KamLAND-ZEN Collaboration [12].

III. TEXTURE ANALYSIS

We undertake the following strategy for the systematic and comprehensive study of the six possible textures of vanishing minors with the collateral condition of vanishing trace.

(i) For a given texture of $C_{ij} = 0$ with vanishing trace $\sum \lambda_i = 0$, we construct Eqs. (12) and (13) with the ratios $\frac{\lambda_2}{\lambda_1} = X$ and $\frac{\lambda_3}{\lambda_1} = Y$. Since Eq. (12) is having the cross term of X and Y, so we have two solutions for each of X and Y. Now there are four options of solution pairs, viz., (X_+, Y_+), (X_+, Y_-), (X_-, Y_+), and (X_-, Y_-) for texture study to be carried out.

(ii) Using the above solution pairs in Eq. (21) via Eqs. (19) and (20), we generate the random numbers for R_ν allowing three mixing angles θ_{12}, θ_{13}, θ_{23} to pick up random numbers in their corresponding 3σ values and the Dirac phase δ in the range 0°–360°. Then we plot R_ν versus δ for normal and inverted mass ordering. If R_ν retains its values within the experimental limits, the texture is considered for further phenomenological study within this allowed range of δ; otherwise, it is rejected. The range of δ so obtained is further checked by plotting the atmospheric mixing angle θ_{23} against δ also for subsequent use.

(iii) With the phenomenologically allowed range of δ obtained via (ii), scatter plots are drawn to find the values of the Majorana phases α and β which may be measured by the experiments in future.

(iv) The viable textures are further explored for the effective Majorana mass of electron neutrino $|m_{ee}|$ indicating the rate of neutrinoless double beta decay and the Jarlskog invariant, J_{cp} representing the strength of CP violation in neutrino oscillations.

To avoid making the paper loaded with a number of plots, now we choose to present the detailed analysis of two textures $C_{11} = 0$ and $C_{12} = 0$ only as representative cases, and the results for other textures shall be summarized in Tables II and III.

A. Case $C_{11} = 0$

For this texture we have

$$A_1 = c^2_{12}c^2_{13}, \tag{24}$$

$$A_2 = s^2_{12}c^2_{13}, \tag{25}$$

$$A_3 = s^2_{13}e^{2i\delta}. \tag{26}$$

Now we first consider the solution pair (X_+, Y_-) to plot R_ν [Eq. (21)] for both NH and IH.

In Fig. 1(a), the ratio R_ν lies within the allowed experimental values that constrain the Dirac phase δ in the range of $(50°, 150°) \oplus (220°, 320°)$ for NH, while in Fig. 1(b) the ratio R_ν lies outside the allowed range, and hence the same texture is phenomenologically ruled out at the 3σ level for IH. Then with the allowed range of δ for NH, the scatter plots are drawn for α and β in Fig. 2. From the plots we obtain the Majorana phases α in the range of $(-25°, 25°)$ and β in $(-45°, 45°)$.

A similar procedure is followed for the solution pairs (X_-, Y_+),(X_+, Y_+), and (X_-, Y_-) of the texture, but plots show that R_ν acquires values far beyond the experimental range. Hence all these solutions of the texture are ruled out.

Now to explore further phenomenology of the texture, $|m_{ee}|$-m_{lightest} and $|m_{ee}|$-β are plotted for neutrinoless double beta decay where the mass of the lightest neutrino is bound within 0.037 eV and 0.042 eV for NH and IH, respectively, at 95% confidence [52]. We also plot J_{cp}-δ for CP violation. From Fig. 3 we observe that $|m_{ee}|$ lies within the experimental bounds, whose results are similar to those in Ref. [53]. Again, in Fig. (4), we find J_{cp} within the range (0.018–0.04). Thus $C_{11} = 0$ is found viable under the phenomenological study for normal mass ordering in the case of the solution pair (X_+, Y_-) of the texture.

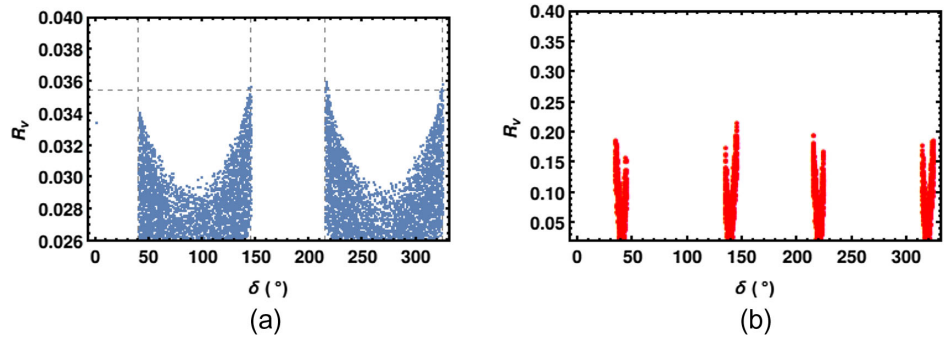

FIG. 1. R_ν plots (a) for NH and (b) for IH.

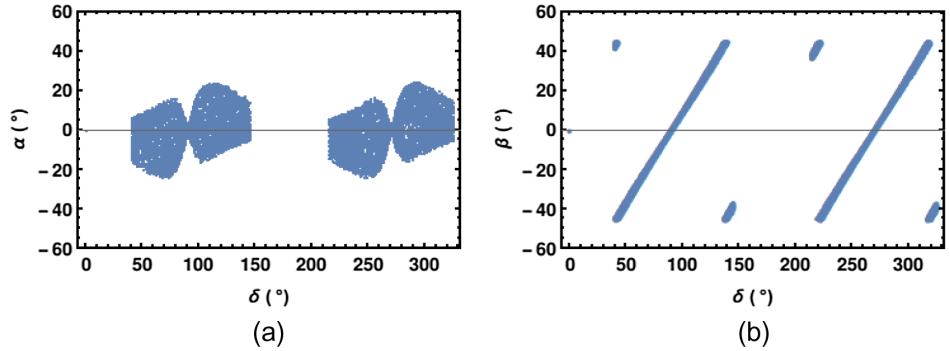

FIG. 2. α and β plots for NH for the pair (X_+, Y_-) with $\delta = (50°, 150°) \oplus (220°, 320°)$.

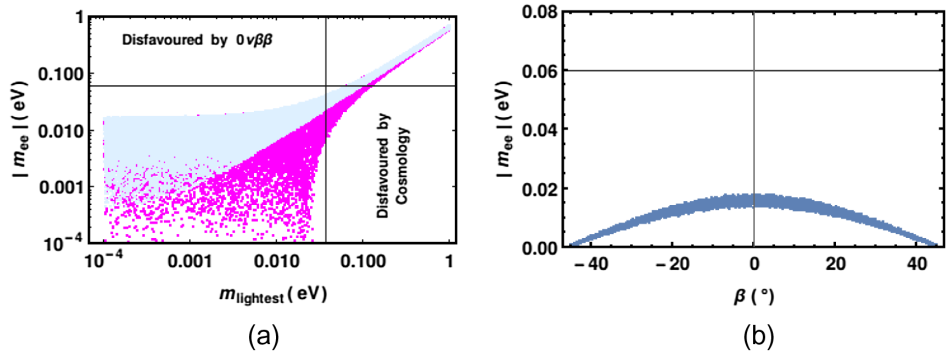

FIG. 3. $|m_{ee}|$ versus m_{lightest} and β plots for (X_+, Y_-) for NH. Region in magenta indicates the experimental bounds, and in light blue shows the allowed region for (X_+, Y_-) for NH.

B. Case $C_{12} = 0$

For this texture A_1, A_2 and A_3 are the following:

$$A_1 = c_{12}s_{12}c_{23}c_{13} + c_{12}^2 c_{13}s_{13}s_{23}e^{-i\delta}, \tag{27}$$

$$A_2 = -c_{12}s_{12}c_{23}c_{13} + s_{12}^2 c_{13}s_{13}s_{23}e^{-i\delta}, \tag{28}$$

$$A_3 = -s_{23}s_{13}c_{13}e^{i\delta}. \tag{29}$$

Now we consider the solution pair (X_+, Y_-) for the texture.

Figure 5 shows that δ is constrained in the range $(20°, 31°) \oplus (45°, 55°) \oplus (128°, 135°) \oplus (148°, 152°) \oplus (225°, 231°) \oplus (300°, 315°) \oplus (331°, 342°)$ for NH. It is found that for IH the ratio R_ν lies outside the allowed experimental range.

On plotting the graphs for α and β in Fig. 6, we obtain $\alpha = (-6°, 6°)$ and $\beta = (-45°, -20°) \oplus (0, 45°)$.

Now we consider the solution pair (X_-, Y_+).

The plot for R_ν in Fig. 7 shows that it lies within the experimental range for $\delta = (82°, 92°) \oplus (270°, 276°)$ for IH only, while the texture is ruled out for NH. In Fig. 8 we

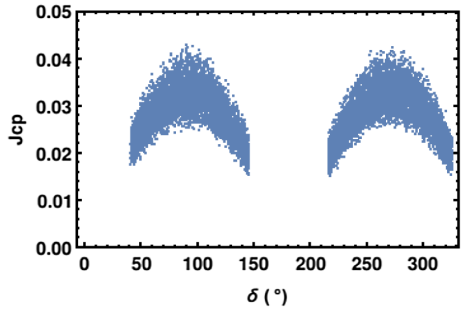

FIG. 4. J_{cp} plot for NH for the solution pair (X_+, Y_-).

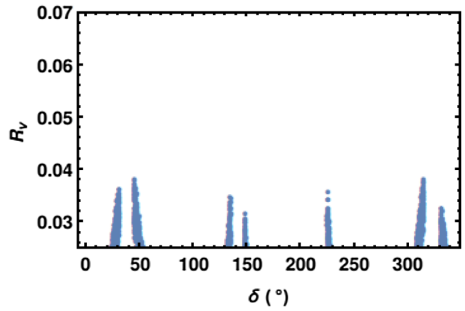

FIG. 5. R_ν plot for NH for the solution pair (X_+, Y_-).

find highly constrained values of α and β as $(-6°, -3°) \oplus (3°, 6°)$ and $(-45°, -35°) \oplus (35°, 45°)$, respectively, for IH.

A similar prescription has been used for the solution pairs (X_+, Y_+) and (X_-, Y_-).

Figure 9 shows that the pairs (X_+, Y_+) and (X_-, Y_-) are viable only for NH in the entire range of δ, i.e., $(0, 360°)$. Figure 10 gives the Majorana phases $\alpha = (-10°, 10°)$ and $\beta = (-50°, 50°)$.

Now we have plotted $|m_{ee}|$, J_{cp}, and θ_{23} for viable cases only in Figs. 11,12, and 13. In Fig. 11, we observe that $|m_{ee}|$ lies within the allowed range, and Fig. 12 gives $J_{cp} = (0.01, 0.04)$ for NH for (X_+, Y_-), (0.023,0.04) for IH for (X_-, Y_+), and (0,0.04) for NH for both (X_+, Y_+) and (X_-, Y_-).

All the remaining textures $C_{13} = 0$, $C_{22} = 0$, $C_{23} = 0$, and $C_{33} = 0$ have been examined following our procedure of analysis. The detailed analyses are not shown in this paper, but the results are presented in Tables II and III. We also checked the atmospheric mixing angle θ_{23} plotted against δ for all other viable textures, and the range is always found in (40°, 45°).

IV. SYMMETRY REALIZATION

The most appealing theoretical approach for generating tiny masses of the light left-handed neutrinos is the seesaw mechanism with the following formula (type I):

$$M_\nu = -M_D M_R^{-1} M_D^T. \tag{30}$$

We carry out a systematic study to realize all the viable textures of M_ν in our present work, by means of the type I seesaw mechanism with an Abelian flavor symmetry. Again, zero textures or vanishing minors of M_ν fundamentally originate from the zero textures M_D and M_R through the seesaw mechanism. It is possible to enforce zero in an arbitrary entry of a fermion mass matrix by means of an Abelian flavor symmetry [40]. We also note that in the lepton sector of the Standard Model, there are three right-handed charged-lepton singlets l_{Ri} and three left-handed lepton doublets, D_{Li}, $(i = 1, 2, 3)$. Further, for the seesaw mechanism, three right-handed neutrino singlets ν_{Ri} are required to be added. Now to build fermion mass matrices M_l, M_D, and M_R under an Abelian flavor symmetry group, for each nonzero entry of M_l or M_D one needs one Higgs doublet, with appropriate transformation properties under the symmetry group, connecting two fermion multiplets corresponding to that entry, and for each nonzero entry of M_R, one requires one scalar singlet with appropriate transfomation properties under the group. Conversely, without admitting a required Higgs doublet or scalar singlet, a zero in an entry of a fermion mass matrix can be enforced.

We present here a detailed analysis of how to realize the structure of the viable neutrino mass matrices presented in

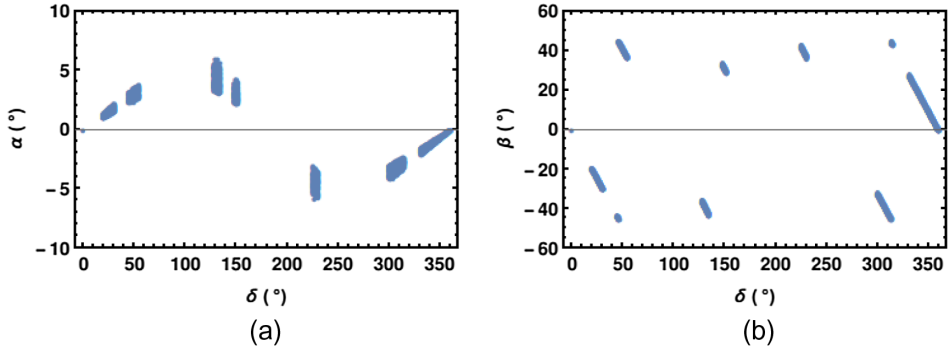

FIG. 6. α and β plots for NH for the solution pair (X_+, Y_-) where δ lies within the range $(20°, 31°) \oplus (45°, 55°) \oplus (128°, 135°) \oplus (148°, 152°) \oplus (225°, 231°) \oplus (300°, 315°) \oplus (331°, 342°)$.

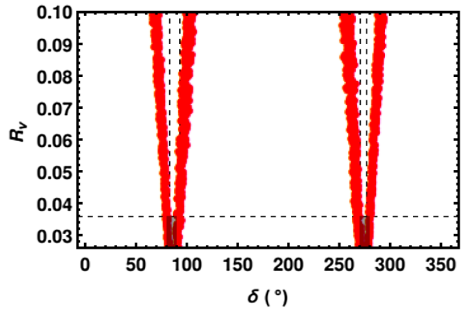

FIG. 7. R_ν plot for IH with the solution pair (X_-, Y_+).

Table II with one vanishing minor. We implement a Z_5 Abelian flavor symmetry group to enforce zeros in fermion mass matrices. A Z_5 consists of the group elements

$$(1, \omega, \omega^2, \omega^3, \omega^4),$$

where $\omega = e^{\frac{i2\pi}{5}}$ is the generator of the group.

Additionally the FN mechanism [42,54] is also augmented to determine the hierarchies between neutrino masses. The FN mechanism is such an appealing approach that can explain the hierarchical structures of quarks and

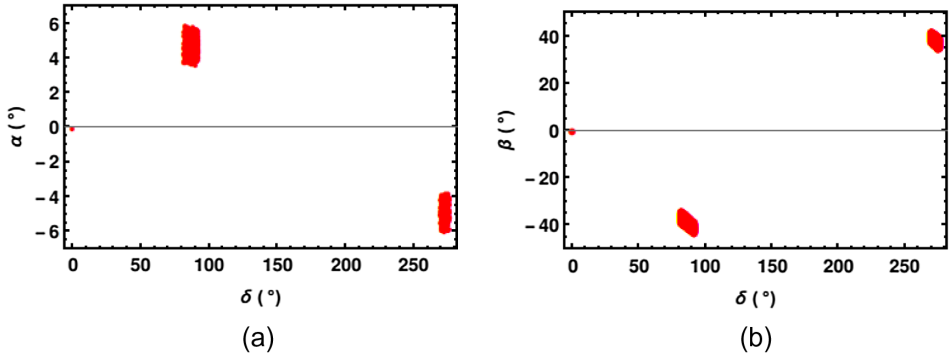

FIG. 8. α and β plots for IH for the solution pair (X_-, Y_+).

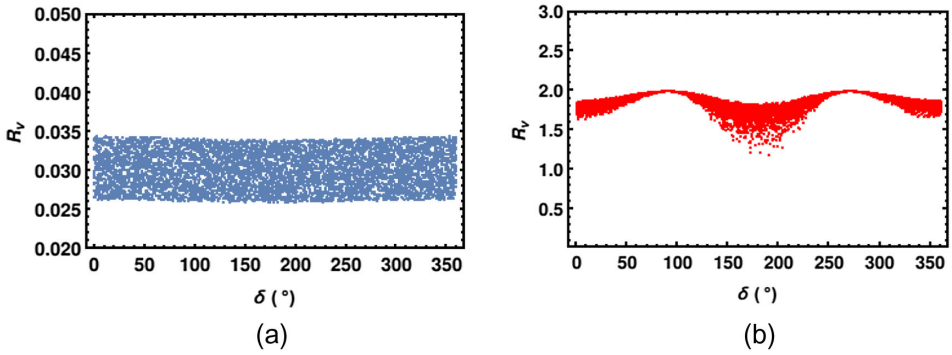

FIG. 9. R_ν plots for both the pairs (X_+, Y_+) and (X_-, Y_-). (a) for NH, and (b) for IH.

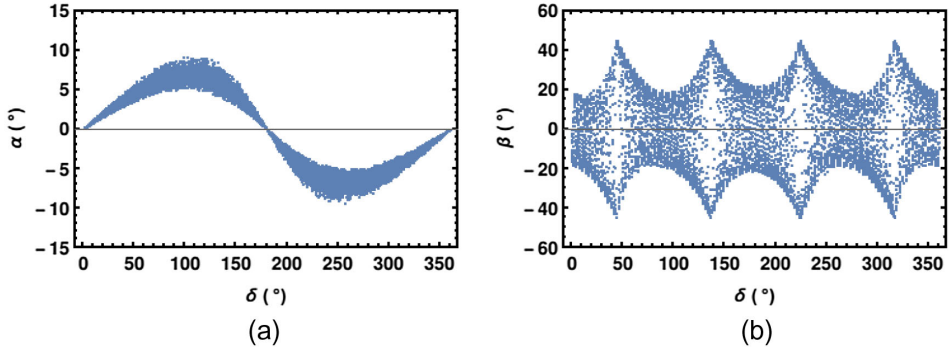

FIG. 10. α and β plots for the pairs (X_+, Y_+) and (X_-, Y_-).

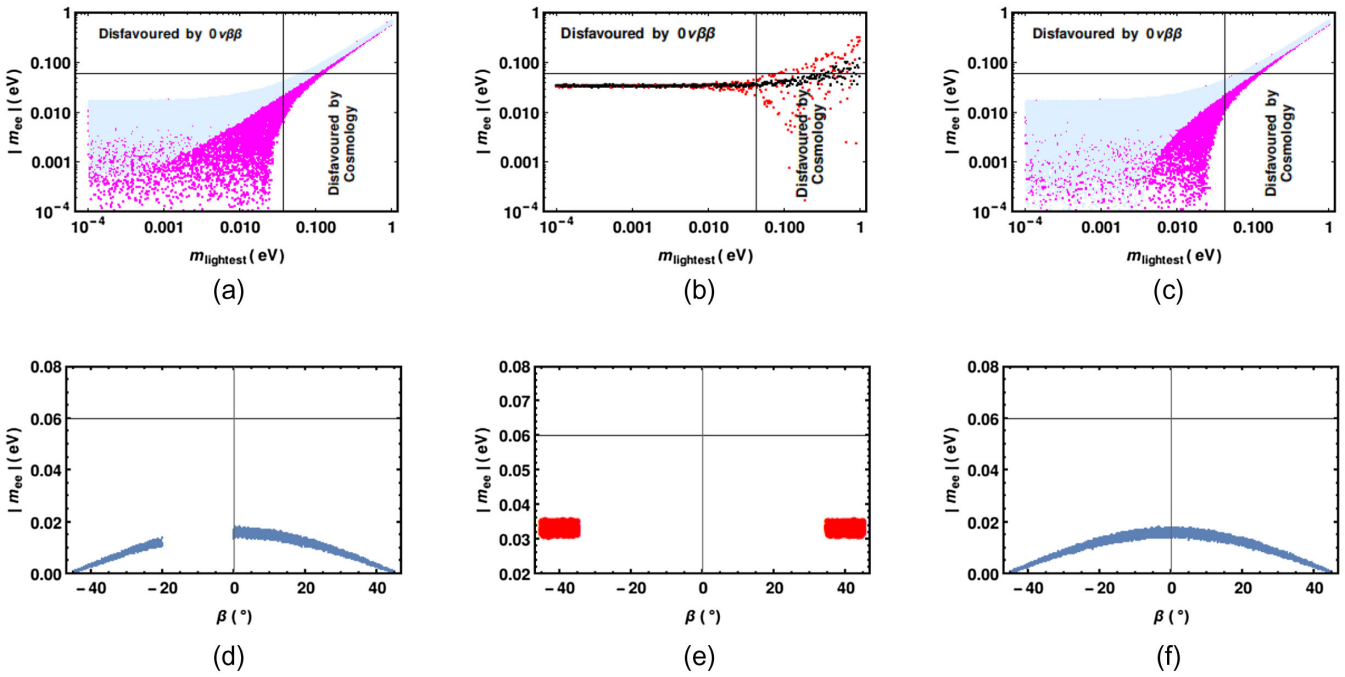

FIG. 11. $|m_{ee}|$ plots for (X_+, Y_-), (X_-, Y_+), $(X_+, Y_+)/(X_-, Y_-)$. The magenta section in (a),(c) and the red area in (b) show the experimental bounds, and the light blue area and black area indicate the allowed range of $|m_{ee}|$ for NH and IH for the solution pairs (X_+, Y_-), (X_-, Y_+), $(X_+, Y_+)/(X_-, Y_-)$.

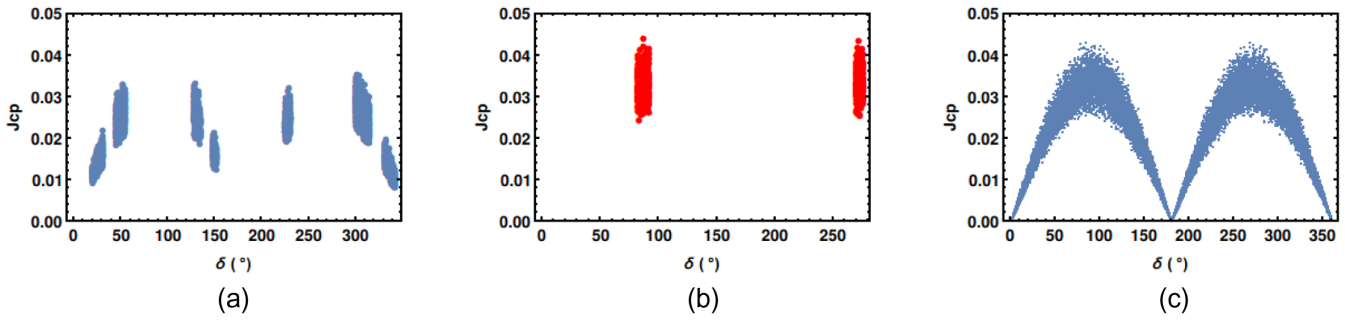

FIG. 12. J_{cp} plots (a), (b), and (c) for (X_+, Y_-), (X_-, Y_+), $(X_+, Y_+)/(X_-, Y_-)$, respectively.

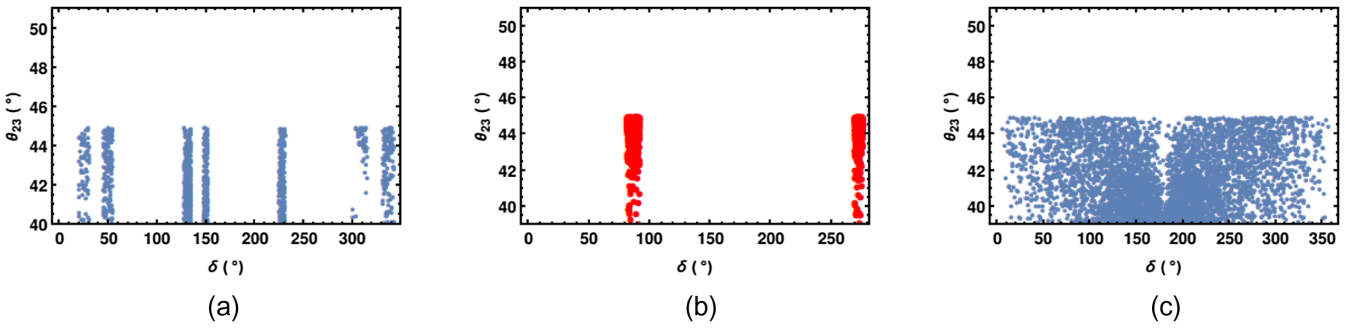

FIG. 13. θ_{23} plots (a), (b), and (c) for (X_+, Y_-), (X_-, Y_+), $(X_+, Y_+)/(X_-, Y_-)$, respectively.

TABLE II. Viable cases under normal hierarchy (NH), inverted hierarchy (IH), and neutrinoless double beta decay.

	(X_+, Y_-)		(X_-, Y_+)		$(X_+, Y_+)/(X_-, Y_-)$		
Case	NH	IH	NH	IH	NH	IH	Neutrinoless double beta decay
C_{11}	✓	✗	✗	✗	✗	✗	All the viable cases are allowed.
C_{12}	✓	✗	✗	✓	✓	✗	
C_{13}	✗	✗	✗	✗	✓	✗	
C_{22}	✓	✗	✓	✗	✗	✗	
C_{23}	✗	✗	✗	✗	✗	✗	
C_{33}	✓	✗	✗	✗	✗	✗	

charged leptons. The basic idea of this mechanism is to introduce $U(1)$ global symmetry and invoke an $SU(2)_L$ singlet scalar field Φ known as a flavon field that acquires the vacuum expectation value (VEV) and breaks the $U(1)$ symmetry. This symmetry breaking is communicated to the fermions so that their effective coupling matrix elements can be expanded in powers of a small positive parameter $\epsilon = \frac{\langle\Phi\rangle}{\Lambda}$ with Λ, the corresponding energy scale of flavor dynamics. Thus the hierarchical textures of fermion masses can intuitively be interpreted as powers of this expansion parameter ϵ. This is the most striking feature of the FN mechanism.

TABLE III. Allowed ranges of CP phases δ, α, β, $|m_{ee}|$, and J_{cp} for the viable cases.

	(X_+, Y_-)		(X_-, Y_+)		$(X_+, Y_+)/(X_-, Y_-)$	
Case	NH	IH	NH	IH	NH	IH
C_{11}	$\delta = (50°, 150°) \oplus (220°, 320°)$	⋯	⋯	⋯	⋯	⋯
	$\alpha = (-25°, 25°)$	⋯	⋯	⋯	⋯	⋯
	$\beta = (-45°, 45°)$	⋯	⋯	⋯	⋯	⋯
	$\lvert m_{ee}\rvert = (0, 0.02)$ eV	⋯	⋯	⋯	⋯	⋯
	$J_{cp} = (0.018, 0.04)$	⋯	⋯	⋯	⋯	⋯
C_{12}	$\delta = (20°, 31°) \oplus (45°, 55°)$ $\oplus (128°, 135°) \oplus (148°, 152°)$ $\oplus (225°, 231°) \oplus (300°, 315°)$ $\oplus (331°, 342°)$	⋯	⋯	$\delta = (82°, 92°)$ $\oplus (270°, 276°)$	$\delta = (0, 360°)$	⋯
	$\alpha = (-6°, 6°)$	⋯	⋯	$\alpha = (3°, 6°)$	$\alpha = (-10°, 10°)$	⋯
		⋯	⋯	$\oplus (-6°, -3°)$		⋯
	$\beta = (-45°, -20°) \oplus (0, 45°)$	⋯	⋯	$\beta = (-45°, -35°)$	$\beta = (-50°, 50°)$	⋯
		⋯	⋯	$\oplus (35°, 45°)$		⋯
	$\lvert m_{ee}\rvert = (0, 0.02)$ eV	⋯	⋯	$\lvert m_{ee}\rvert = (0.03, 0.035)$ eV	$\lvert m_{ee}\rvert = (0, 0.02)$ eV	⋯
	$J_{cp} = (0.01, 0.04)$	⋯	⋯	$J_{cp} = (0.023, 0.04)$	$J_{cp} = (0, 0.04)$	⋯
C_{13}		⋯	⋯	⋯	$\delta = (55°, 130°)$	⋯
		⋯	⋯	⋯	$\oplus (230°, 310°)$	⋯
	⋯	⋯	⋯	⋯	$\alpha = (-9°, -3°)$	⋯
	⋯	⋯	⋯	⋯	$\oplus (3°, 9°)$	⋯
	⋯	⋯	⋯	⋯	$\beta = (-50°, 50°)$	⋯
	⋯	⋯	⋯	⋯	$\lvert m_{ee}\rvert = (0, 0.02)$ eV	⋯
	⋯	⋯	⋯	⋯	$J_{cp} = (0, 0.04)$	⋯
C_{22}	$\delta = (40°, 90°) \oplus (230°, 279°)$	⋯	$\delta = (0, 30°) \oplus (196°, 210°)$	⋯	⋯	⋯
	$\oplus (310°, 350°)$		$\oplus (290°, 335°)$	⋯	⋯	⋯
	$\alpha = (-45°, -35°) \oplus (0, 45°)$	⋯	$\alpha = (-45°, 45°)$	⋯	⋯	⋯
	$\beta = (-45°, 45°)$	⋯	$\beta = (-50°, 50°)$	⋯	⋯	⋯
	$\lvert m_{ee}\rvert = (0, 0.02)$ eV	⋯	$\lvert m_{ee}\rvert = (0, 0.02)$ eV	⋯	⋯	⋯
	$J_{cp} = (0, 0.04)$	⋯	$J_{cp} = (0, 0.04)$	⋯	⋯	⋯
C_{33}	$\delta = (90°, 265°)$	⋯	⋯	⋯	⋯	⋯
	$\alpha = \beta = (-45°, 45°)$	⋯	⋯	⋯	⋯	⋯
	$\lvert m_{ee}\rvert = (0, 0.02)$ eV	⋯	⋯	⋯	⋯	⋯
	$J_{cp} = (0, 0.04)$	⋯	⋯	⋯	⋯	⋯

The Lagrangian which is responsible for the generation of the lepton masses and the hierarchy of the mass matrices arising from the FN mechanism can be written as

$$\begin{aligned}\mathcal{L} = &\left(\frac{\langle\Phi\rangle}{\Lambda}\right)^{Q_{D_{Li}}+Q_{l_{Rj}}} Y_{ij}^{(k)} \bar{D}_{Li}\phi_k l_{Rj} \\ &+ \left(\frac{\langle\Phi\rangle}{\Lambda}\right)^{Q_{D_{Li}}+Q_{\nu_{Rj}}} Y_{ij}^{(k)} \bar{D}_{Li}\tilde{\phi}_k \nu_{Rj} \\ &+ \left(\frac{\langle\Phi\rangle}{\Lambda}\right)^{Q_{\nu_{Ri}}+Q_{\nu_{Rj}}} Y_{ij}^{(k)} \chi_k \bar{\nu}_{Ri}\nu_{Rj} + \text{H.c.} \end{aligned} \tag{31}$$

The $Q_\alpha(\alpha = D_L, l_R, \nu_R)$ are the FN charges for the Standard Model (SM) fermion ingredients under which different generations may be charged differently. The flavon Φ obtains the VEV$\langle\Phi\rangle$ that breaks the FN symmetry. For all the cases, we assign the FN charges for the Lepton sector as

$$\begin{aligned}\bar{D}_{L1,2,3}&:(a+1, a, a),\\ l_{R1,2,3}&:(0, 1, 2),\\ \nu_{R1,2,3}&:(d, c, b).\end{aligned}$$

Here a comment is in order. The tracelessness of M_ν does not speak much about the texture of M_ν (e.g., possible zeros) which is supposed to be the result of some deeper theory [41]. On the other hand, the vanishing minor results from the seesaw mirroring between M_ν and M_R with diagonal M_D [54]. Thus one zero texture of M_R with diagonal M_D manifests as vanishing minor of the corresponding element of M_ν, and hence the symmetry realization under Z_N is actionable for the vanishing minor only.

A. Symmetry realization for $C_{11} = 0$

We consider the following M_R and M_D for vanishing minor of the (1,1) element of M_ν.

$$M_R = \begin{pmatrix} 0 & \xi & \zeta \\ \xi & \eta & \upsilon \\ \zeta & \upsilon & \kappa \end{pmatrix}, \qquad M_D = \begin{pmatrix} x & 0 & 0 \\ 0 & y & 0 \\ 0 & 0 & z \end{pmatrix},$$

$$\begin{aligned} M_\nu &= -M_D M_R^{-1} M_D^T \\ &= \frac{1}{\Gamma}\begin{pmatrix} (-\upsilon^2+\eta\kappa)x^2 & (\zeta-\xi y)xy & (-\zeta\eta+\xi\upsilon)xz \\ (\zeta-\xi y)xy & -\zeta^2 y^2 & \xi\zeta yz \\ (-\zeta\eta+\xi\upsilon)xz & \xi\zeta yz & -\xi^2 z^2 \end{pmatrix}, \end{aligned} \tag{32}$$

where $\Gamma = -\zeta\eta^2 + 2\xi\zeta\upsilon - \xi^2\kappa$.

On implementing Z_5 symmetry, the fields of the relevant particles transform as

$$\begin{aligned} &\nu_{R1} \to \omega^3\nu_{R1}, \quad \bar{D}_{L1} \to \omega^2\bar{D}_{L1}, \quad l_{R1} \to \omega^3 l_{R1} \\ &\nu_{R2} \to \omega^2\nu_{R2}, \quad \bar{D}_{L2} \to \omega^3\bar{D}_{L2}, \quad l_{R2} \to \omega^2 l_{R2} \\ &\nu_{R3} \to \nu_{R3}, \quad \bar{D}_{L3} \to \bar{D}_{L3}, \quad l_{R3} \to l_{R3} \end{aligned} \tag{33}$$

Here $D_{Li}, l_{Rj}, \nu_{Ri}, (i, j = 1, 2, 3)$ represents the $SU(2)_L$ doublets, the right-handed (RH) $SU(2)_L$ singlets, and the right-handed (RH) neutrino singlets, respectively.

Forming the required bilinears dictated by Z_5 symmetry we obtain

$$\nu_{Ri}^T\nu_{Rj} = \begin{pmatrix} \omega & 1 & \omega^3 \\ 1 & \omega^4 & \omega^2 \\ \omega^3 & \omega^2 & 1 \end{pmatrix}, \quad \bar{D}_{Li}\nu_{Rj} = \begin{pmatrix} 1 & \omega^4 & \omega^2 \\ \omega & 1 & \omega^3 \\ \omega^3 & \omega^2 & 1 \end{pmatrix},$$
$$\bar{D}_{Li}l_{Rj} = \begin{pmatrix} 1 & \omega^4 & \omega^2 \\ \omega & 1 & \omega^3 \\ \omega^3 & \omega^2 & 1 \end{pmatrix}.$$

We consider the transformation of the singlet scalars χ_k $(k = 1, 2, 3)$ which is responsible for the Majorana neutrino mass matrix M_R, and SM-like doublet scalar ϕ which is responsible for the Dirac neutrino mass matrix M_D, and the lepton mass matrix M_l under Z_5 transformation as

$$\begin{aligned} &\chi_1 \to \omega^2\chi_1, \quad \chi_2 \to \omega^3\chi_2, \quad \chi_3 \to \omega\chi_3 \\ &\phi \to \phi. \end{aligned} \tag{34}$$

Now the Lagrangian dictated by Z_5 is

$$\begin{aligned}\mathcal{L}_M^{Z_5} = &\epsilon^{d+c} m_{12}\nu_{R1}^T c^{-1}\nu_{R2} + \epsilon^{d+b} Y_{\chi_{13}}^{(1)}\chi_1\nu_{R1}^T c^{-1}\nu_{R3} + \epsilon^{2c} Y_{\chi_{22}}^{(3)}\chi_3\nu_{R2}^T c^{-1}\nu_{R2} + \epsilon^{c+b} Y_{\chi_{23}}^{(2)}\chi_2\nu_{R2}^T c^{-1}\nu_{R3} \\ &+ \epsilon^{2b} m_{33}\nu_{R3}^T c^{-1}\nu_{R3} + \epsilon^{a+d+1} Y_{D_{11}}\bar{D}_{L1}\tilde{\phi}\nu_{R1} + \epsilon^{a+c} Y_{D_{22}}\bar{D}_{L2}\tilde{\phi}\nu_{R2} + \epsilon^{a+b} Y_{D_{33}}\bar{D}_{L3}\tilde{\phi}\nu_{R3} \\ &+ \epsilon^{a+1} Y_{l_{11}}\bar{D}_{L1}\phi l_{R1} + \epsilon^{a+1} Y_{l_{22}}\bar{D}_{L2}\phi l_{R2} + \epsilon^{a+2} Y_{l_{33}}\bar{D}_{L3}\phi l_{R3}. \end{aligned} \tag{35}$$

Now we construct the mass matrix M_R, M_D, and M_l as

$$M_R = \begin{pmatrix} 0 & \epsilon^{d+c} m_{12} & y^{(1)}_{\chi_{13}} \chi_1 \epsilon^{d+b} \\ \epsilon^{d+c} m_{12} & y^{(3)}_{\chi_{22}} \chi_3 \epsilon^{2c} & y^{(2)}_{\chi_{23}} \chi_2 \epsilon^{c+b} \\ y^{(1)}_{\chi_{13}} \chi_1 \epsilon^{d+b} & y^{(2)}_{\chi_{23}} \chi_2 \epsilon^{c+b} & \epsilon^{2b} m_{33} \end{pmatrix}, \tag{36}$$

$$M_D = \begin{pmatrix} y_{D_{11}} \tilde{\phi} \epsilon^{a+d+1} & 0 & 0 \\ 0 & y_{D_{22}} \tilde{\phi} \epsilon^{a+c} & 0 \\ 0 & 0 & y_{D_{33}} \tilde{\phi} \epsilon^{a+b} \end{pmatrix}, \qquad M_l = \begin{pmatrix} y_{l_{11}} \phi \epsilon^{a+1} & 0 & 0 \\ 0 & y_{l_{22}} \phi \epsilon^{a+1} & 0 \\ 0 & 0 & y_{l_{33}} \phi \epsilon^{a+2} \end{pmatrix}. \tag{37}$$

We get the effective neutrino mass matrix M_ν using seesaw mechanism $M_\nu = -M_D M_R^{-1} M_D^T$ as

$$M_\nu = \Omega \begin{pmatrix} \epsilon^2 \tilde{\phi}^2 y^2_{D_{11}} (y^{(2)2}_{\chi_{23}} \chi_2^2 - m_{33} y^{(3)}_{\chi_{22}} \chi_3) & \epsilon \tilde{\phi}^2 y_{D_{11}} y_{D_{22}} (m_{11} m_{33} - y^{(1)}_{\chi_{13}} y^{(2)}_{\chi_{23}} \chi_1 \chi_2) & -\epsilon \tilde{\phi}^2 y_{D_{11}} y_{D_{33}} (m_{11} y^{(2)}_{\chi_{23}} \chi_2 - y^{(1)}_{\chi_{13}} y^{(3)}_{\chi_{22}} \chi_1 \chi_3) \\ \epsilon \tilde{\phi}^2 y_{D_{11}} y_{D_{22}} (m_{11} m_{33} - y^{(1)}_{\chi_{13}} y^{(2)}_{\chi_{23}} \chi_1 \chi_2) & \tilde{\phi}^2 y^2_{D_{22}} y^{(1)2}_{\chi_{13}} \chi_1^2 & -m_{11} \tilde{\phi}^2 y_{D_{22}} y_{D_{33}} Y^{(1)}_{\chi_{13}} \chi_1 \\ -\epsilon \tilde{\phi}^2 y_{D_{11}} y_{D_{33}} (m_{11} y^{(2)}_{\chi_{23}} \chi_2 - y^{(1)}_{\chi_{13}} y^{(3)}_{\chi_{22}} \chi_1 \chi_3) & -\tilde{\phi}^2 y_{D_{22}} y_{D_{33}} Y^{(1)}_{\chi_{13}} \chi_1 m_{11} & \tilde{\phi}^2 y^2_{D_{33}} m^2_{11} \end{pmatrix}, \tag{38}$$

where $\Omega = \frac{\epsilon^{2a}}{m^2_{11} m_{33} - y^{(1)}_{\chi_{13}} \chi_1 (2 m_{11} y^{(2)}_{\chi_{23}} \chi_2 - y^{(1)}_{\chi_{13}} y^{(3)}_{\chi_{22}} \chi_1 \chi_3)}$.

B. Symmetry realization for $C_{12} = 0$

$$M_R = \begin{pmatrix} \gamma & 0 & \zeta \\ 0 & \eta & \upsilon \\ \zeta & \upsilon & \kappa \end{pmatrix}, \qquad M_D = \begin{pmatrix} x & 0 & 0 \\ 0 & y & 0 \\ 0 & 0 & z \end{pmatrix},$$
$$M_\nu = \frac{1}{\Psi} \begin{pmatrix} (-\upsilon^2 + \eta\kappa) x^2 & \zeta \upsilon x y & -\zeta \eta x z \\ \zeta \upsilon x y & (-\zeta^2 + \gamma\kappa) y^2 & -\gamma \upsilon y z \\ -\zeta \eta x z & -\gamma \upsilon y z & \gamma \eta z^2 \end{pmatrix}, \tag{39}$$

where $\Psi = -\zeta\eta^2 - \gamma\upsilon^2 + \gamma\eta\kappa$. The transformations of the relevant particle fields under Z_5 are shown in Table IV.

C. Symmetry realization for $C_{13} = 0$

$$M_R = \begin{pmatrix} \gamma & \xi & 0 \\ \xi & \eta & \upsilon \\ 0 & \upsilon & \kappa \end{pmatrix}, \qquad M_D = \begin{pmatrix} x & 0 & 0 \\ 0 & y & 0 \\ 0 & 0 & z \end{pmatrix},$$

TABLE IV. Symmetry transformation for $C_{12} = 0$.

Symmetry under Z_5					
$\nu_{R1} \to \nu_{R1}$	$\nu_{R2} \to \omega^2 \nu_{R2}$	$\nu_{R3} \to \omega^3 \nu_{R3}$	$\bar{D}_{L1} \to \bar{D}_{L1}$	$\bar{D}_{L2} \to \omega^3 \bar{D}_{L2}$	$\bar{D}_{L3} \to \omega^2 \bar{D}_{L3}$
$l_{R1} \to l_{R1}$	$l_{R2} \to \omega^2 l_{R2}$	$l_{R3} \to \omega^3 l_{R3}$	$\chi_1 \to \omega^2 \chi_1$	$\chi_2 \to \omega \chi_2$	$\chi_3 \to \omega^4 \chi_3$
$\phi \to \phi$					

TABLE V. Symmetry transformation for $C_{13} = 0$.

Symmetry under Z_5					
$\nu_{R1} \to \omega\nu_{R1}$	$\nu_{R2} \to \nu_{R2}$	$\nu_{R3} \to \omega^3\nu_{R3}$	$\bar{D}_{L1} \to \omega^4\bar{D}_{L1}$	$\bar{D}_{L2} \to \bar{D}_{L2}$	$\bar{D}_{L3} \to \omega^2\bar{D}_{L3}$
$l_{R1} \to \omega l_{R1}$	$l_{R2} \to l_{R2}$	$l_{R3} \to \omega^3 l_{R3}$	$\chi_1 \to \omega^3\chi_1$	$\chi_2 \to \omega^4\chi_2$	$\chi_3 \to \omega^2\chi_3$
$\phi \to \phi$					

TABLE VI. Symmetry transformation for $C_{22} = 0$.

Symmetry under Z_5					
$\nu_{R1} \to \omega^2\nu_{R1}$	$\nu_{R2} \to \omega^3\nu_{R2}$	$\nu_{R3} \to \omega\nu_{R3}$	$\bar{D}_{L1} \to \omega^3\bar{D}_{L1}$	$\bar{D}_{L2} \to \omega^2\bar{D}_{L2}$	$\bar{D}_{L3} \to \omega^4\bar{D}_{L3}$
$l_{R1} \to \omega^2 l_{R1}$	$l_{R2} \to \omega^3 l_{R2}$	$l_{R3} \to \omega l_{R3}$	$\chi_1 \to \omega\chi_1$	$\chi_2 \to \omega^2\chi_2$	$\chi_3 \to \omega^3\chi_3$
$\phi \to \phi$					

$$M_\nu = \frac{1}{\Sigma}\begin{pmatrix} (-\upsilon^2 + \eta\kappa)x^2 & -\xi\kappa xy & \xi\upsilon xz \\ -\xi\kappa xy & \gamma\kappa y^2 & -\gamma\upsilon yz \\ \xi\upsilon xz & -\gamma\upsilon yz & (-\xi^2 + \gamma\eta)z^2 \end{pmatrix}, \tag{40}$$

where $\Sigma = -\gamma\upsilon^2 - \xi^2\kappa + \gamma\eta\kappa$. The transformations of the relevant particle fields under Z_5 are shown in Table V.

D. Symmetry realization for $C_{22} = 0$

$$M_R = \begin{pmatrix} \gamma & \xi & \zeta \\ \xi & 0 & \upsilon \\ \zeta & \upsilon & \kappa \end{pmatrix}, \qquad M_D = \begin{pmatrix} x & 0 & 0 \\ 0 & y & 0 \\ 0 & 0 & z \end{pmatrix},$$

$$M_\nu = \frac{1}{\Delta}\begin{pmatrix} -\upsilon^2 x^2 & (\zeta\upsilon - \xi\kappa)xy & \xi\upsilon xz \\ (\zeta\upsilon - \xi\kappa)xy & (-\zeta^2 + \gamma\kappa)y^2 & (\xi\zeta - \gamma\upsilon)yz \\ \xi\upsilon xz & (\xi\zeta - \gamma\upsilon)yz & -\xi^2 z^2 \end{pmatrix}, \tag{41}$$

where $\Delta = 2\xi\zeta\upsilon - \gamma\upsilon^2 - \xi\kappa^2$. The transformations of the relevant particle fields under Z_5 are shown in Table VI.

E. Symmetry realization for $C_{33} = 0$

$$M_R = \begin{pmatrix} \gamma & \xi & \zeta \\ \xi & \eta & \upsilon \\ \zeta & \upsilon & 0 \end{pmatrix}, \qquad M_D = \begin{pmatrix} x & 0 & 0 \\ 0 & y & 0 \\ 0 & 0 & z \end{pmatrix},$$

$$M_\nu = \frac{1}{\Pi}\begin{pmatrix} -\upsilon^2 x^2 & \zeta\upsilon xy & (-\zeta\eta + \xi\upsilon)xz \\ \zeta\upsilon xy & -\zeta^2 y^2 & (\xi\zeta - \gamma\upsilon)yz \\ (-\zeta\eta + \xi\upsilon)xz & (\xi\zeta - \gamma\upsilon)yz & (-\xi^2 + \gamma\eta)z^2 \end{pmatrix}, \tag{42}$$

where $\Pi = -\zeta^2\eta + 2\xi\zeta\upsilon - \gamma\upsilon^2$. The transformations of the relevant particle fields under Z_5 are shown in Table VII.

TABLE VII. Symmetry transformation for $C_{33} = 0$.

Symmetry under Z_5					
$\nu_{R1} \to \nu_{R1}$	$\nu_{R2} \to \omega\nu_{R2}$	$\nu_{R3} \to \omega^2\nu_{R3}$	$\bar{D}_{L1} \to \bar{D}_{L1}$	$\bar{D}_{L2} \to \omega^4\bar{D}_{L2}$	$\bar{D}_{L3} \to \omega^3\bar{D}_{L3}$
$l_{R1} \to l_{R1}$	$l_{R2} \to \omega l_{R2}$	$l_{R3} \to \omega^2 l_{R3}$	$\chi_1 \to \omega^4\chi_1$	$\chi_2 \to \omega^3\chi_2$	$\chi_3 \to \omega^2\chi_3$
$\phi \to \phi$					

For all the viable cases we obtain

$$M_\nu \sim \epsilon^{2a}\begin{pmatrix} \epsilon^2 & \epsilon & \epsilon \\ \epsilon & 1 & 1 \\ \epsilon & 1 & 1 \end{pmatrix}. \tag{43}$$

The texture of M_ν indicates normal hierarchy with $\mu - \tau$ symmetry, i.e., $\theta_{13} = 0$ and the maximal atmospheric mixing $\theta_{23} = \frac{\pi}{4}$. To achieve experimentally viable textures, broken $\mu - \tau$ symmetry and deviation from maximal atmospheric mixing can be done by appropriate perturbation in the neutrino mass matrix.

V. RESULTS AND DISCUSSION

In this work, we have carried out a phenomenological texture study of the Majorana neutrino mass matrices with the Ansätze of one vanishing minor and the zero sum of the eigenvalues with the *CP* phases. One of the two simultaneous constraint equations consists of the cross term of the variables, so we had the option of four solution pairs of the equations. Interestingly the solution pairs have interplay in various possible textures under study. The systematic numerical analysis has been carried out with the latest 3σ neutrino oscillation data. Although the current neutrino oscillation data shed some light on the range of the Dirac *CP* phase δ, the Majorana *CP* phases α and β are still completely unexplored. As the prime objective of this work, to step in such an unknown terrain of neutrinos, we have strategized to find out the phenomenologically allowed values of the Majorana *CP* phases α and β for different viable textures. We have also explored the neutrinoless double beta decay rate $|m_{ee}|$ and the strength of *CP* violation J_{cp} for all viable textures. The ranges of α, β, δ, $|m_{ee}|$, and J_{cp} in our study have been summarized in Table III.

To understand the origin of zeros in fermion mass matrices, we have implemented a Z_5 flavor symmetry group. Again to get the information of hierarchy of the viable textures, additionally the FN mechanism was augmented. The symmetry realization is an important work for realistic model building.

Now we summarize our observations of this texture study as follows:

(i) The viability of the textures was checked on the basis of the values of δ within the values of the ratio of the mass-squared difference R_ν both at the 3σ level. In this context, the textures $C_{11} = 0$, $C_{13} = 0$, $C_{22} = 0$, and $C_{33} = 0$ have been found viable for normal hierarchy only, and the case $C_{12} = 0$ has been found viable for both normal and inverted hierarchies. Again the case $C_{23} = 0$ is completely ruled out. Interestingly the solution pair (X_+, Y_-) from our Ansätze supports all the cases except the case $C_{13} = 0$. The solution pairs (X_+, Y_+) and (X_-, Y_-) support the cases $C_{12} = 0$ and $C_{13} = 0$ for normal hierarchy. Further the solution pair (X_-, Y_+) supports $C_{12} = 0$ for inverted hierarchy and $C_{22} = 0$ for normal hierarchy. The interplay of the solution pairs exists in the results.

(ii) The Majorana phase α for the textures $C_{12} = 0$ and $C_{13} = 0$ is vanishingly small, and the range is highly constrained.

(iii) For all the viable textures, the atmospheric mixing angle θ_{23} lies in the range (40°, 45°). Thus the phenomenology of these textures favors the first quadrant for atmospheric mixing.

(iv) For all the cases both the neutrinoless double beta decay rate $|m_{ee}|$ and the strength of the Dirac *CP* violation J_{CP} remain within the experimental bounds.

(v) Symmetry realization of all the viable textures has been done under the discrete symmetry group Z_5. Additionally the FN mechanism has been augmented to check the hierarchy of the textures. We have found that all the cases favor the normal hierarchy of the neutrino mass pattern.

Finally, we expect that our numerical results of the Dirac and Majorana *CP* phases may be verified in the future neutrino experiments designed for that purpose.

ACKNOWLEDGMENTS

One of the authors, S. D., has acknowledged the funding support for this work from the Department of Science and Technology (DST), India (Grant No. DST/INSPIRE, Fellowship No. /2018/IF180713) under the scheme of the INSPIRE fellowship program.

[1] P. Adamson, I. Anghel, A. Aurisano, G. Barr, M. Bishai, A. Blake, G. Bock, D. Bogert, S. Cao, C. Castromonte *et al.*, Phys. Rev. Lett. **112**, 191801 (2014).

[2] K. Abe, N. Abgrall, Y. Ajima, H. Aihara, J. Albert, C. Andreopoulos, B. Andrieu, S. Aoki, O. Araoka, J. Argyriades *et al.*, Phys. Rev. Lett. **107**, 041801 (2011).

[3] D. Ayres *et al.* (NOvA Collaboration), arXiv:hep-ex/0503053.

[4] F. An, J. Bai, A. Balantekin, H. Band, D. Beavis, W. Beriguete, M. Bishai, S. Blyth, K. Boddy, R. Brown *et al.*, Phys. Rev. Lett. **108**, 171803 (2012).

[5] J. K. Ahn, S. Chebotaryov, J. Choi, S. Choi, W. Choi, Y. Choi, H. Jang, J. Jang, E. Jeon, I. Jeong *et al.*, Phys. Rev. Lett. **108**, 191802 (2012).

[6] F. An, G. An, Q. An, V. Antonelli, E. Baussan, J. Beacom, L. Bezrukov, S. Blyth, R. Brugnera, M. B. Avanzini *et al.*, J. Phys. G **43**, 030401 (2016).

[7] H.-K. Proto-Collaboration, K. Abe, H. Aihara, C. Andreopoulos, I. Anghel, A. Ariga, T. Ariga, R. Asfandiyarov, M. Askins, J. Back *et al.*, Prog. Theor. Exp. Phys. **2015**, 053C02 (2015).

[8] B. Abi, R. Acciarri, M. Acero, G. Adamov, D. Adams, M. Adinolfi, Z. Ahmad, J. Ahmed, T. Alion, S. A. Monsalve *et al.*, Eur. Phys. J. C **80**, 978 (2020).

[9] J. Wolf (for the KATRIN Collaboration), Nucl. Instrum. Methods Phys. Res., Sect. A **623**, 442 (2010).

[10] I. Abt, M. Altmann, A. Bakalyarov, I. Barabanov, C. Bauer, E. Bellotti, S. Belyaev, L. Bezrukov, V. Brudanin, C. Buettner *et al.*, arXiv:hep-ex/0404039.

[11] M. Danilov, R. DeVoe, A. Dolgolenko, G. Giannini, G. Gratta, P. Picchi, A. Piepke, F. Pietropaolo, P. Vogel, J. Vuilleumier *et al.*, Phys. Lett. B **480**, 12 (2000).

[12] A. Gando, Y. Gando, T. Hachiya, A. Hayashi, S. Hayashida, H. Ikeda, K. Inoue, K. Ishidoshiro, Y. Karino, M. Koga *et al.*, Phys. Rev. Lett. **117**, 082503 (2016).

[13] L. Lavoura, Phys. Lett. B **609**, 317 (2005).

[14] E. Lashin and N. Chamoun, Phys. Rev. D **78**, 073002 (2008).

[15] E. Lashin and N. Chamoun, Phys. Rev. D **80**, 093004 (2009).

[16] S. Dev, S. Verma, S. Gupta, and R. R. Gautam, Phys. Rev. D **81**, 053010 (2010).

[17] S. Verma, Nucl. Phys. **B854**, 340 (2012).

[18] S. Dev, S. Gupta, R. R. Gautam, and L. Singh, Phys. Lett. B **706**, 168 (2011).

[19] J. Liao, D. Marfatia, and K. Whisnant, Phys. Rev. D **89**, 013009 (2014).

[20] H. Fritzsch, Z.-z. Xing, and S. Zhou, J. High Energy Phys. 09 (2011) 083.

[21] J. Barranco, D. Delepine, and L. Lopez-Lozano, Phys. Rev. D **86**, 053012 (2012).

[22] J. Liao, D. Marfatia, and K. Whisnant, Phys. Rev. D **87**, 073013 (2013).

[23] J. Liao, D. Marfatia, and K. Whisnant, Phys. Rev. D **88**, 033011 (2013).

[24] L. Lavoura, W. Rodejohann, and A. Watanabe, Phys. Lett. B **726**, 352 (2013).

[25] R. R. Gautam, M. Singh, and M. Gupta, Phys. Rev. D **92**, 013006 (2015).

[26] J. Liao, D. Marfatia, and K. Whisnant, Nucl. Phys. **B900**, 449 (2015).

[27] T. Kitabayashi, Phys. Rev. D **102**, 075027 (2020).

[28] R. R. Gautam, Phys. Rev. D **97**, 055022 (2018).

[29] P. H. Frampton, S. L. Glashow, and D. Marfatia, Phys. Lett. B **536**, 79 (2002).

[30] Z.-z. Xing, Phys. Lett. B **530**, 159 (2002).

[31] S. Dev, S. Verma, and S. Gupta, Phys. Lett. B **687**, 53 (2010).

[32] S. Dev, R. R. Gautam, and L. Singh, Phys. Rev. D **87**, 073011 (2013).

[33] S. Dev, S. Gupta, and R. R. Gautam, Phys. Rev. D **82**, 073015 (2010).

[34] S. Kaneko, H. Sawanaka, and M. Tanimoto, J. High Energy Phys. 08 (2005) 073.

[35] X.-G. He and A. Zee, Phys. Rev. D **68**, 037302 (2003).

[36] M. Singh, Adv. High Energy Phys. **2018**, 2863184 (2018).

[37] G. C. Branco, R. G. Felipe, F. Joaquim, and T. Yanagida, Phys. Lett. B **562**, 265 (2003).

[38] W. Rodejohann, Phys. Lett. B **579**, 127 (2004).

[39] W. Grimus, Proc. Sci. HEP2005 (**2006**) 186.

[40] W. Grimus, A. S. Joshipura, L. Lavoura, and M. Tanimoto, Eur. Phys. J. C **36**, 227 (2004).

[41] D. Black, A. H. Fariborz, S. Nasri, and J. Schechter, Phys. Rev. D **62**, 073015 (2000).

[42] C. D. Froggatt and H. B. Nielsen, Nucl. Phys. **B147**, 277 (1979).

[43] J. Han, R. Wang, W. Wang, and X.-N. Wei, Phys. Rev. D **96**, 075043 (2017).

[44] W. Wang, Eur. Phys. J. C **73**, 2551 (2013).

[45] C. Jarlskog, Phys. Rev. Lett. **55**, 1039 (1985).

[46] C. Arnaboldi, D. Artusa, F. Avignone III, M. Balata, I. Bandac, M. Barucci, J. Beeman, C. Brofferio, C. Bucci, S. Capelli *et al.*, Phys. Lett. B **584**, 260 (2004).

[47] L. Gironi, C. Arnaboldi, J. Beeman, O. Cremonesi, F. Danevich, V. Y. Degoda, L. Ivleva, L. Nagornaya, M. Pavan, G. Pessina *et al.*, J. Instrum. **5**, P11007 (2010).

[48] C. E. Aalseth, D. Anderson, R. Arthur, F. Avignone III, C. Baktash, T. Ball, A. S. Barabash, F. Bertrand, R. L. Brodzinski, V. Brudanin *et al.*, Nucl. Phys. B, Proc. Suppl. **138**, 217 (2005).

[49] A. Barabash, Nucl. Phys. B, Proc. Suppl. **221**, 26 (2011).

[50] H. V. Klapdor-Kleingrothaus *et al.*, Eur. Phys. J. A **12**, 147 (2001).

[51] M. C. Gonzalez-Garcia, M. Maltoni, and T. Schwetz, Universe **7**, 459 (2021).

[52] P. Stöcker, C. Balázs, S. Bloor, T. Bringmann, T. E. Gonzalo, W. Handley, S. Hotinli, C. Howlett, F. Kahlhoefer, J. J. Renk *et al.*, Phys. Rev. D **103**, 123508 (2021).

[53] P. Chen, S. C. Chuliá, G.-J. Ding, R. Srivastava, and J. W. Valle, Phys. Rev. D **98**, 055019 (2018).

[54] Z.-z. Xing, Phys. Rep. **854**, 1 (2020).